Copyright © 2012 American Scientific Publishers
All rights reserved
Printed in the United States of America

Journal of
Nanoscience and Nanotechnology
Vol. 12, 5930–5936, 2012

RESEARCH ARTICLE

Synthesis of Pt Doped Bi_2O_3/RuO_2 Photocatalysts for Hydrogen Production from Water Splitting Using Visible Light

S. H. Hsieh[1], G. J. Lee[1], C. Y. Chen[2], J. H. Chen[3], S. H. Ma[3], T. L. Horng[4], K. H. Chen[5], and J. J. Wu[1,*]

[1] *Department of Environmental Engineering and Science,* [2] *Department of Material Science and Engineering,* [3] *Department of Photonics,* [4] *Department of Applied Mathematics,* [5] *Department of Electrical Engineering, Feng Chia University, Taichung 407, Taiwan*

This study was focused on the preparation of modified bismuth oxide photocatalysts, including Ru and Pt doped Bi_2O_3, using sonochemically assisted method to enhance their photocatalytic activity. The crystalline phase composition and surface structure of Bi_2O_3 photocatalysts were examined using SEM, XRD, UV-visible spectroscopy, and XPS. Optical characterizations have indicated that the Bi_2O_3 presents the photoabsorption properties shifting from UV light region into visible light which is approaching towards the edge of 470 nm. According to the experimental results, visible-light-driven photocatalysis for water splitting with the addition of 0.3 M Na_2SO_3 and 0.03 M $H_2C_2O_4$ as sacrificing agents demonstrates that Pt/Bi_2O_3-RuO_2 catalyst could increase the amount of hydrogen evolution, which is around 11.6 and 14.5 μmol g^{-1} h^{-1}, respectively. Plausible formation mechanisms of modified bismuth oxide and reaction mechanisms of photocatalytic water splitting have been proposed.

Keywords: Nano Photocatalyst, Water Splitting, Hydrogen Production, Bismuth Oxide.

1. INTRODUCTION

Since global population has been predicted to increase by a factor of 36% to 8.9 billion by the year of 2050, the issue of providing affordable, reliable, and environmentally sustainable energy to the world's population has become a major challenge for the first half of this century and beyond. With such uncertain supply of energy in the world today, the cost of oil has increased significantly in the past few years.[1] In addition, alternative fuels are not available and most of these fuels require a different engine technology for efficient operation.[2] Therefore, growing environmental concerns related to the extensive use of non-sustainable fossil fuels, including oil, natural gas, and coal, and an increasing energy demand will accelerate mankind, sooner or later, adopt clean and sustainable sources of energy.[3] In addition, fossil fuels have been related to the issue of global warming. Since atmospheric CO_2 concentration has increased from 280 ppm in the 1700 s to 380 ppm in 2005, at a progressively faster rate each decade,[4,5] scientists are looking for renewable resources that are plentiful and beneficial to our environment. Recently, there has been much attention on the development of hydrogen technologies as a potential solution to the current energy crisis. Although many hydrogen technologies have been developed currently, solar photocatalytic water splitting is thought to be a potential way for hydrogen production due to no contamination in the process. Photocatalytic water splitting to generate hydrogen and oxygen simultaneously using semiconductors has received remarkable attentions recently. Since the work of Honda and Fujishima on the decomposition of water using TiO_2 as the photocatalyst in 1972,[6] many researches on the conversion of solar energy to chemical energy have been directed towards the development of photocatalytic systems which are capable of splitting water into hydrogen and oxygen.[7,8] In this research, we prepared stable nano-sized bismuth oxide-based semiconductors, i.e., Bi_2O_3 and Bi_2O_3-RuO_2, due to narrower bandgap at 2.8 eV which would allow to respond the visible light with the wavelength less than 443 nm. In addition, sacrificial reagents were used to react with electrons and holes to increase the rate of hydrogen production. The major purpose was to

*Author to whom correspondence should be addressed.

 1533-4880/2012/12/5930/007 doi:10.1166/jnn.2012.6396

experimentally optimize the water decomposition at efficient production rate of hydrogen as a potential clean fuel.

2. EXPERIMENTAL DETAILS

In the study, all chemicals were purchased from Aldrich Company and used without further purification.

2.1. Synthesis of Bi_2O_3 and Bi_2O_3-RuO_2 Catalysts

6g $Bi(NO_3)_3$ was dissolved in 7.5 mL 1 M HNO_3 to obtain Bi^{3+} aqueous solution, to which 4 g polyvinyl pyrrolidone (PVP) was added as a dispersant. 10% Ruthenium trichloride ($RuCl_3 \cdot 3H_2O$) was used as a precursor and added to synthesize Bi_2O_3-RuO_2 catalyst. Sodium hydroxide (4 M) was poured into the Bi^{3+} aqueous solution under vigorous stirring condition. The pH value was about 12 and immediately resulted in the formation of white precipitates in the beaker. After stirring for several minutes, the mixture was then applied with high-intensity ultrasound (600 W, 20 kHz) for 30 minutes. During the irradiation, the temperature of the reaction mixture rose to 60 °C and the color of the suspension mixture changed from white to yellowish. After irradiation, the precipitates were centrifuged and washed by alcohol and deionized water for several times, and then dried at 60 °C in a vacuumed oven to obtain the final faint yellow Bi_2O_3 and Bi_2O_3-RuO_2 samples, which were then calcined at 500 °C for 2 hours.

2.2. Synthesis of Pt/Bi_2O_3-RuO_2

Pt nanoparticles were anchored using photochemical deposition on the surface of Bi_2O_3-RuO_2 photocatalyst. The Bi_2O_3-RuO_2 catalyst (150 mg) was dispersed in 100 mL of distilled water by ultrasonic agitation for 1 hour. Following sonication, the slurry was transferred into the reactor and a solution of 1:1 (v/v) water-methanol was added so that the final volume was about 50 mL. Subsequently, the required amount of aqueous solution of $H_2PtCl_6 \cdot 6H_2O$ for platinum precursor was added while the suspension was stirred vigorously by a magnetic stirrer. The suspension was then irradiated with a PenRay UV lamp (wavelength at 254 nm) for two hours to allow sufficient deposition of most metals. After irradiation, the Pt/Bi_2O_3-RuO_2 catalyst was filtered and washed several times to remove excess chloride ions, and dried it overnight at 80 °C.

2.3. Evaluation of Photocatalytic Activity for Hydrogen Production from Water Splitting

Photocatalytic reactions were conducted using the catalysts as prepared in Section 2.2. The reactant solution, consisting of 0.2 g Pt/Bi_2O_3:RuO_2 and 200 ml of pure water, was purged with helium to ensure no air remained inside the reactor. The evolved gases, including hydrogen and oxygen) were monitored and analyzed by a gas chromatograph connected directly to the closed gas-circulation system. The photocatalytic water splitting with the addition of 0.03 M oxalic acid and 0.3 M sodium sulphite, respectively, was carried out using visible light irradiation at controlled condition. Before turning on the visible light, helium was purged through the reactor by removing oxygen prior to photocatlysis reaction. The photocatalysts were irradiated by a 350 W Xe lamp which allowed visible light to pass using a cut-off filter ($\lambda \geqq 400$ nm). The amounts of hydrogen and oxygen gases were determined using gas chromatography (Shumadzu 17A) equipped with thermal conductivity detector (TCD).

3. RESULTS AND DISCUSSION

The synthesis of Bi_2O_3 was performed via hydrolysis and precipitation with bismuth ions as the precursors. Surfactant polyvinylpyrrolidone (PVP) plays a significant role to control the particle size and size distribution of Bi_2O_3 as-synthesized. The stabilizing PVP would coordinate to metal ions before the reduction and this interaction provided a different growth pathway leading to the formation of nanorods.[9] Since the viscosity of solution increases significantly with adding PVP, it restricts the diffusion and growth process associated with the nanocrystal formation. Based on the tendency, the addition of PVP surfactant has strong effects on the grain sizes and morphologies of Bi_2O_3. In our preliminary experiment (data not shown), the addition of PVP up to 4 g was found to produce the smallest size of catalysts as prepared. However, PVP dose more than 4 g would not improve the catalyst size at all. Subsequently, the hydrolysis product $Bi(OH)_3$ is dehydrated into Bi_2O_3 by ultrasound-assisted sonolysis. When bismuth hydroxide precursor was irradiated with high intensity ultrasound, acoustic cavitations could randomly provide very high temperatures and pressures to increase the chance of collisions between nuclei particles. In this study, the formation route of Bi_2O_3 nanocrystal synthesized by ultrasound sonolysis is shown in Figure 1. In the initial stage, tiny crystalline nuclei are generated in the supersaturated solution and grow into nanosheets. When PVP is added into the Bi^{3+} solution, the aggregation occurs between bismuth ions. Due to the high concentration of bismuth ions, it can inhibit the growth rate of crystal and lead nanosheets to stick with each other.

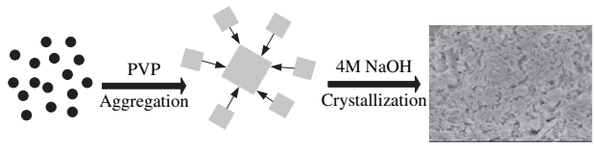

Fig. 1. Schematic routes of Bi_2O_3 synthesis.

Delivered by Ingenta to:
National Chung Hsing University
IP: 140.120.25.65
Thu, 04 Oct 2012 11:43:44

RESEARCH ARTICLE

3.1. Characterization of Photocatalysts

XRD was used to investigate the phase structures of the catalyst samples. The XRD patterns of Bi_2O_3 and Bi_2O_3-RuO_2 are shown in Figures 2(a), (b). All the intensive and sharp diffraction peaks could be perfectly indexed to α-Bi_2O_3 (JCPDS: 71-2274). It indicated that well-crystallized α-Bi_2O_3 nanoparticles were successfully prepared using sonochemical method at room temperature. The α-Bi_2O_3 is a stable low-temperature polymorph, which was reported to be monoclinic, and the polymorph formed at high temperature is cubic δ-Bi_2O_3 that is stable only between ca. 730 °C. The unit cell parameter was calculated as the value of $a = 5.848$ Å, $b = 8.166$ Å, and $c = 7.509$ Å. Three main peaks of Bi_2O_3 at 27.4°, 33.3°, and 46.3° corresponded to (121), (122), and (041), respectively. No other impurity diffraction peaks were detected, indicating that precursors have been completely transformed into the Bi_2O_3 phase. From Figure 2(a), it can be found to match with the cubic phase of Bi_2O_3. The intensity of peaks is lower than Bi_2O_3 with ruthenium doping as shown in Figure 2(b). The presence of weak peaks is indexed to primitive-cubic of $Bi_3Ru_3O_{11}$ (JCPDS: 73-2380). Thus, ruthenium doped Bi_2O_3 has been successfully prepared using sonolysis. In Figure 2(c), the XRD analysis indicated the presence of Pt and Bi_2O_3 composite. Additional weak diffraction peaks of other phases were not present, which indicated that no other crystalline impurities were observed. In addition, the XRD spectra of all Pt modified catalysts were analyzed. The characteristic peaks of the monoclinic structure (JCPDS Card File No. 71-2274) with the strong characteristic peaks (121), (122), (041) are noted for the Bi_2O_3 sample. The weak characteristic peaks of powders with 2 wt% Pt loading can be indexed to face-centered-cubic (fcc) Pt (111), (200), (311) corresponding to $2\theta = 40.2°$, 46.8°, and 82.4°, respectively (JCPDS Card File No. 87-0647). However, such results appear that Pt loading on the Bi_2O_3 composites surface is relatively scarce.

The Bi_2O_3 prepared via sonochemical synthesis possesses fiber-like morphologies as shown in Figures 3(a) and (b). Upon clear examination of SEM image, we notice that the fiber-like morphology (60–70%) consists of fiber particles. In addition to fiber-like morphologies of bismuth oxide, many nanosheets are also produced. It is also noted that the structure is similar to rod morphology and grows along the ends from the center to form 1D nanorod. Such high energy using ultrasonic irradiation might provide Bi_2O_3 with a high degree of crystallinity assembled as shown in Figures 3(c) and (d). Therefore, it is obvious to obtain the fiber-like appearance using high concentration of bismuth oxide, which has been corresponded with the SEM images. The high resolution TEM (HRTEM) images were also observed as the fiber. Furthermore, many dots on the edge indicated the presence of PVP, which would influence the particle size of Bi_2O_3.

The growth processes of Bi_2O_3 were investigated at different reaction time. Figure 4 shows a series of SEM images of products by extending the reaction time from 60 min, 120 min, up to 180 min under sonolysis. On shorter reaction period (1 h), SEM images (Fig. 4(a)) revealed that the product consisted of large rods (ca. ~500 nm in diameter and ~2 μm in length). When reaction time increased, short rods (ca. ~200 nm is diameter and ~1 μm in length) in bismuth oxides (Fig. 4(b)) was recorded. After 180 min (Fig. 4(c)) of reaction time, the size of bismuth oxides was figured out the smallest and the morphologies were composed of fibers and nanosheets. In general, reaction time may enhance the crystal growth by the accumulation of energy. However, the crystal growth is substantially suppressed in our study due to the violent collision between particles under high energy intensity of ultrasound.

Delivered by Ingenta to:
National Chung Hsing University
IP: 140.120.25.6
Thu, 04 Oct 2012 01:13:44

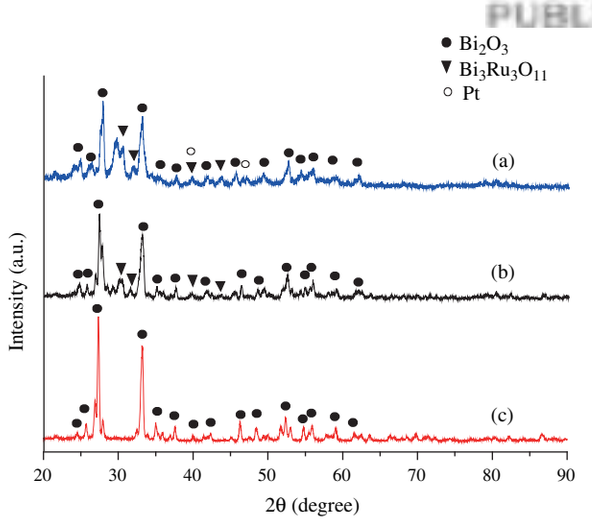

Fig. 2. XRD pattern of (a) Pt/Bi_2O_3-RuO_2, (b) Bi_2O_3-RuO_2, and (c) Bi_2O_3 prepared in the solution with PVP.

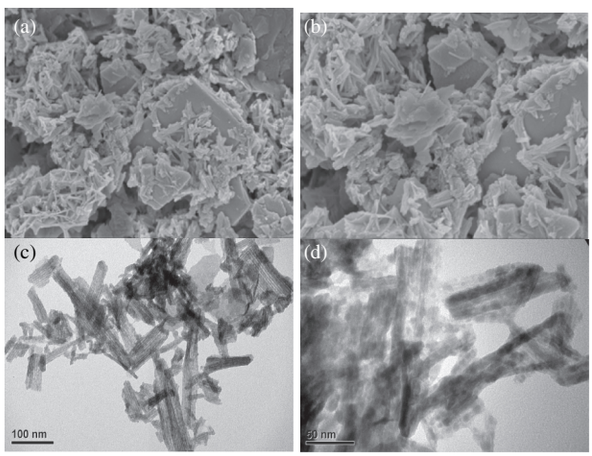

Fig. 3. SEM image of (a and b) and TEM image of (c and d) of Bi_2O_3.

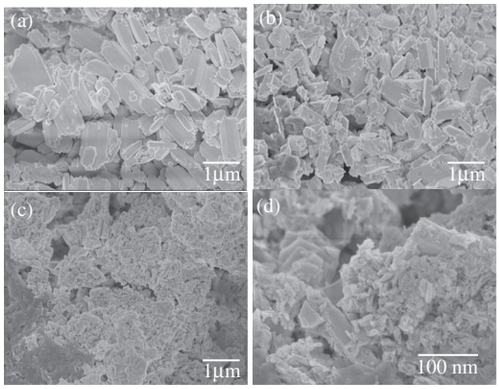

Fig. 4. Effect of reaction time for (a) 1 h, (b) 2 h and (c and d) 3 h on Bi_2O_3 nanorod under high-intensity ultrasound.

When the concentration of $Bi(NO_3)_3$ was fixed at 0.5 mol L^{-1} and the reaction temperature was kept at 60 °C for 3 h, the as-produced Bi_2O_3 were measured with a mean crystal size of 44.7 nm via submicron particle size analyzer. The particle size distribution of Bi_2O_3 is seen in Figure 5. In order to enhance its activity as a photocatalyst, much effort has been attempted to modify Bi_2O_3 by doping with ruthenium. In this study, bismuth oxide was doped by ruthenium around 10 mol%. The specific surface area of Bi_2O_3 (22.7 m^2/g) becomes larger with doping more ruthenium oxide, of which the specific surface area of Bi_2O_3-RuO_2 is 41.66 m^2/g.

In order to obtain Bi_2O_3 nanoparticles, the minimum reaction temperature was found to be 60 °C by sonolysis and excessive NaOH should be dosed into the mixture of $Bi(NO_3)_3$ solution. Monodispersed particles are favorable to form when the nucleation rate is much higher than that of the particle growth. In the present synthesis procedure, the sudden addition of excessive NaOH has made the concentration of $Bi(OH)_{3-n}$ species become critical supersaturation, resulting in eruptible nucleation.[10] The reaction processes in aqueous solution can be summarized in the following Eqs. (1) to (3):

$$Bi^{3+} + H_2O + NO_3^- \rightarrow BiONO_3 \downarrow + 2H^+ \quad (1)$$

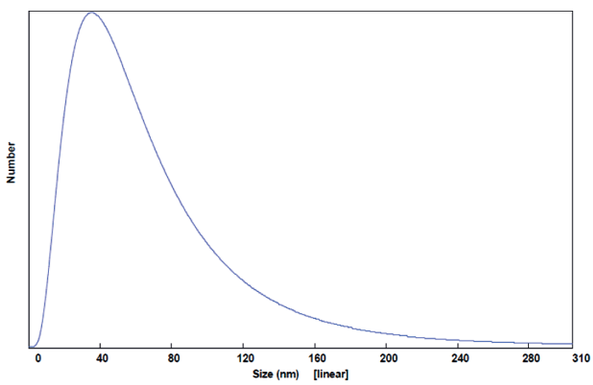

Fig. 5. The particle size distribution of as-synthesized Bi_2O_3.

$$2BiONO_3 + 2OH^- \rightarrow Bi(OH)^n_{3-n} + 2NO_3^- + H_2O \quad (2)$$

$$2Bi(OH)^n_{3-n} \rightarrow Bi_2O_3 \downarrow + 3H_2O \quad (3)$$

$Bi(NO_3)_3$ is first hydrolyzed in water to produce slightly soluble $BiONO_3$ [Eq. (1)].[11] When excess NaOH is added in the solution, Bi_2O_3 will appear immediately due to the fast reaction rate of $BiONO_3$ and OH^- under the present reaction condition as shown in Eq. (2). Large quantities of OH^- can force the Eqs. (2) and (3) shift towards the right side while the pH value increases. On the other hand, the surfactant (PVP) acting as a dispersant is thought to slow down the diffusion rate of solutes onto the crystal surfaces of the as-formed nuclei, which ensures that the diffusion process can dominate the rate-control step during the crystal growth procedure.[12] To understand the growth mechanism of the Bi_2O_3 structure, the growth processes were systematically studied by analyzing the samples at different growth stage. Crystal growth by aggregation can occur by two means, including random aggregation and the oriented attachment mechanism. One dimensional nanorods or nanoribbons can further self-attach by planar van der Waals interactions or lateral "lattice fusion" to generate either length-multiplied one-dimensional nanostructures or two-dimensional crystal sheets and walls.[13] According to the Bi_2O_3 (0.5 mole L^{-1}) results, the growth route is proposed by two primary mechanisms after fast nucleation in solution, such as the Ostwal ripening process and the aggregation growth process. Crystal growth by aggregation occurs by the oriented attachment mechanism due to the formation of bismuth oxide with rod morphology. In this study, ultrasound could destroy the large rods and inhibit the aggregation of $Bi(OH)_3$. Subsequently, it self-assembles to produce larger particles with high concentration (0.5 mole L^{-1}), which may decrease the growth rate of crystal and lead to the formation of nanosheets.

The FTIR spectrum (data not shown) of the as-synthesized Bi_2O_3 nanoparticle was performed and the vibration absorption bands due to NO_3^- (1383.96 cm^{-1}) and Bi–O–Bi (825.29 cm^{-1}) were substantially observed. This suggests that the Bi_2O_3 nanospheres contain a large amount of NO_3^- groups on their surfaces, which are crucial for further surface functionalization and coating by any other functional groups or organic/inorganic components.[14] The spectra also display a strong absorption band in the 544.00–424.00 cm^{-1} range, which is due to Bi–O stretching mode. This phenomenon is in an agreement with the data reported by Carrazan et al.,[15] where they indicated the range of 600.00–400.00 cm^{-1} and the stretching and deformation modes involving Bi–O modes were expected. The absorption band at 424, 508, and 544 cm^{-1} in FTIR spectra are assigned to α-Bi_2O_3.[16]

3.2. Optical Properties of Photocatalysts

To better understand the chemical states of the catalysts, XPS spectra analysis was performed in this research. The

Delivered by Ingenta to:
National Chung Hsing University
IP: 140.120.22.6
Fri, 07 Oct 2012 01:13:44

RESEARCH ARTICLE

binding energies were corrected for specimen charging by reference C1s peak at 284.8 eV. The quantitative analysis was done using XPS spectra obtained at the depth of about 50 nm from the surface. Figure 6 shows XPS wide scans for the Pt/Bi_2O_3-RuO_2 catalyst, and elements of Bi, O, Ru, and Pt. It reveals that all the Bi species in the Bi_2O_3-RuO_2 sample are present in the form of Bi_2O_3, corresponding to the binding energy of Bi_2O_3 (158.6 eV and 163.9 eV) in Bi ($4f_{7/2}$) and Bi ($4f_{5/2}$) levels, respectively.[17] The peaks locating at 157.1 and ∼162.4 eV can be attributed to the binding energies of Bi $4f_{7/2}$ and Bi $4f_{5/2}$, respectively, in element Bi, while the peaks at ∼159.1 and ∼164.4 eV can be assigned to Bi_2O_3.[18] According to Yao et al.,[19] XPS represents an electronic interaction between the ZnO and PVP phases in ZnO/PVP nanocomposite. The binding energy of Zn $2p_{3/2}$ was shifted negatively from 1021.4 eV (pure ZnO) down to 1021.0 eV in the ZnO/PVP sample. These observations suggested a charge-transfer from the PVP to the ZnO. The XPS spectra in Figure 6(b) have demonstrated that the Bi species in Bi_2O_3-RuO_2 sample is present in pure Bi_2O_3 phase. According to the above mentioned phenomena, the binding energy has blue shift due to the interactions between Bi_2O_3, PVP, and Ru. In addition, Figure 6(c) shows that the XPS Ru ($3d_{5/2}$) is located at 280.4 eV with a spin orbit splitting $3d_{5/2}$–$3d_{3/2}$ of 4.1 eV. Chen et al.[20] has figured out that the [Ru^{4+}] peaks, identified as $3d_{5/2}$ and $3d_{3/2}$ at 280.3 and 284.5 eV, are attributed to the 4+ oxidation state of ruthenium. Their results are supportive to our observance, which are at 280.4 and 284.6 eV, respectively. The peak at 280.5 eV shows a large contribution from Ru metal because it has a binding energy of 280.0–280.3 eV and no other stable Ru cations with oxidation state lower than +4 are known to exist in the solid state.

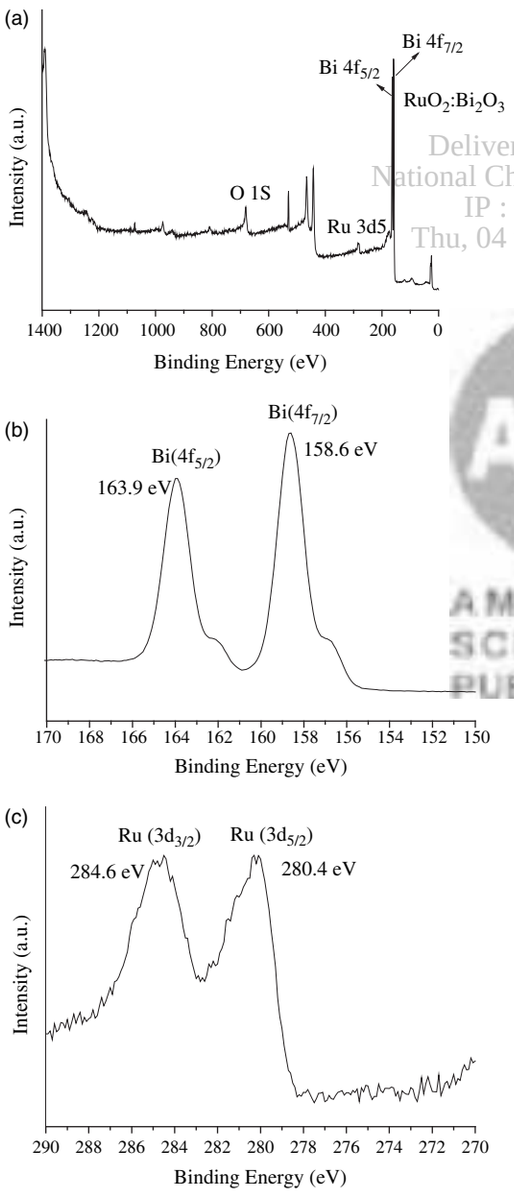

Fig. 6. XPS spectra for (a) Bi_2O_3-RuO_2, (b) Bi_{4f} for Bi_2O_3-RuO_2, and (c) Ru_{3d} for Bi_2O_3-RuO_2.

Delivered by Ingenta to:
National Chung Hsing University
IP : 140.120.25.83
Thu, 04 Oct 2012 01:13:44

3.3. Photocatalytic Activity for Hydrogen Production

Figure 7 shows the H_2 evolution from 0.3 M Na_2SO_3 and 0.03 M $H_2C_2O_4$ solution under visible light illumination. The formation amounts of H_2 are estimated to be 24.3, 30.3, 39.5, and 46.4 μmol g^{-1}, and 27.6, 35.6, 47.2, and 58 μmol g^{-1} by the addition of 0.3 M Na_2SO_3 and 0.03 M $H_2C_2O_4$, respectively, in 4 hours for commercial Bi_2O_3, Bi_2O_3, Bi_2O_3-RuO_2, and Pt/Bi_2O_3-RuO_2. The production rate of H_2 increases on Pt/Bi_2O_3-RuO_2 and Bi_2O_3-RuO_2, but decreases on commercial Bi_2O_3 photocatalysts than that of as-synthesized Bi_2O_3. It is noted that the activity of commercial Bi_2O_3 is the lowest, where the H_2 evolution rate is about 6.1 and 6.9 μmol g^{-1} h^{-1} for 0.3 M Na_2SO_3 and 0.03 M $H_2C_2O_4$. Since the particle size of commercial Bi_2O_3 (∼10 μm) is larger than as-synthesized Bi_2O_3 (∼100 nm) and its specific surface area is also smaller (commercial Bi_2O_3: 0.02 m^2/g; Bi_2O_3: 22.7 m^2/g), commercial bismuth oxide cannot offer more activity for water splitting during photocatalytic reactions compared with bismuth oxide synthesized in the study. Besides, bismuth oxide semiconductor has the band-gap energy of 2.8 eV and its major absorption limit is at or below 443 nm. In order to make it as a good visible light responsible catalyst, bismuth oxide might be sensitized "internally" by doping with transition metal ions. Ruthenium oxide doped Bi_2O_3 has been found to enhance the amount of hydrogen evolution as shown in Figures 7(a) and (b). It is because doping ruthenium ion will form the donor level within the energy band that can diminish e^-/h^+ recombination. On the other hand, Bi_2O_3-RuO_2 also has small particle size (∼100 nm), the distance that photogenerated electrons and

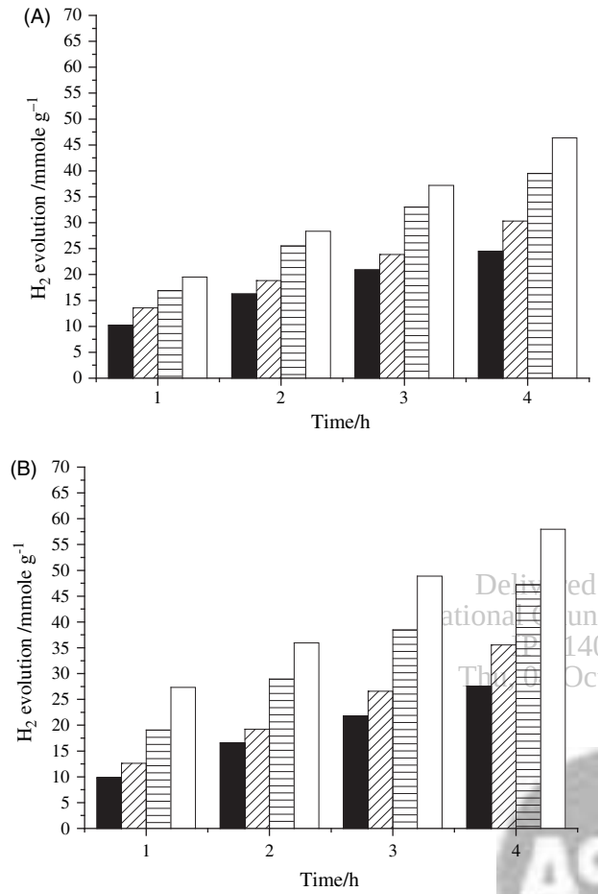

Fig. 7. Hydrogen production by visible-light-driven photocatalysts with (a) 0.3 M Na_2SO_3 (b) 0.03 M $H_2C_2O_4$. (■) commercial Bi_2O_3, (▨) Bi_2O_3, (▤) Bi_2O_3-RuO_2 (□) Pt/Bi_2O_3-RuO_2.

holes migrating to reaction site on the surface becomes short and leads to a decrease in recombination probability by active sites or photocatalytic reaction center. Nevertheless, the hydrogen rate could be further increased to 11.6 μmol g^{-1} h^{-1} using Pt/Bi_2O_3-RuO_2 catalyst when 2 wt% Pt was loaded on the surface of Bi_2O_3/RuO_2. Pt loading on the photocatalyst surface has been recognized to effectively enhance the photocatalytic activity of the composite. When the loaded Pt is less than 2 wt%, the photocatalytic activity of photocatalyst can be intensified with increased Pt.[21] From the result, we can conclude that Pt nanoparticle plays an important role in hydrogen production and Pt clusters act as a separation center. The positive effect of Pt deposition is due to the fact that Pt nanoparticles on the semiconductor surface behave like electron traps, which provide sites for the accumulation of photoexcited electrons, and then improve the separation of photoexcited electrons and holes. Although Pt/Bi_2O_3-RuO_2 exhibits the best photocatalytic activity for overall water splitting, back reaction of water might suppress the hydrogen production due to rapid water formation on the Pt nanoparticles. In addition, the photocatalytic water splitting using two different sacrificial reagents has indicated that the hydrogen production rate by 0.03 M $H_2C_2O_4$ is better than 0.3 M Na_2SO_3 due to more negative potential of $H_2C_2O_4$ than Na_2SO_3 by easily providing electrons or reducing species to the holes. Additionally, the Na_2SO_3 solution is alkaline and less hydrogen ions can initiate the hydrogen formation although the surfaces of as-synthesized photocatalysts are negatively charged in the alkaline solution that is somehow easier to attract H^+ onto the surface of photocatalysts.

4. CONCLUSIONS

Fiber-like Bi_2O_3 photocatalyst has been successfully synthesized using sonochemical method at the temperature of 60 °C. The concentration of bismuth ions and reaction time are important factors to determine the size and morphology of Bi_2O_3, which can be attributed to different reaction routes. XRD analysis appears that α-phase of Bi_2O_3 is formed and well-crystallized Bi_2O_3 particles can be produced. The maximum rates of hydrogen evolution, 11.6 and 14.5 μmol g^{-1} h^{-1}, are obtained using Pt/Bi_2O_3-RuO_2 photocatalyst for water splitting with the addition of 0.3 M Na_2SO_3 and 0.03 M $H_2C_2O_4$, respectively.

Acknowledgments: This study was acknowledged by the financial support from the National Science Council (NSC) in Taiwan under contract number of 100-2632-E-035-001-MY3 and New-star project from Feng Chia University.

References and Notes

1. U.S. Department of Energy, Hydrogen, Fuel Cells and Infrastructure Technologies Program, Hydrogen Posture Plan, U.S. **(2006)**.
2. J. D. Holladay, J. Hu, D. L. King, and Y. Wang, *Catal. Today* 139, 244 **(2009)**.
3. J. Zhu and M. Zäch, *Curr. Opin. Colloid Interface Sci.* 14, 260 **(2009)**.
4. D. M. Etheridge, L. P. Steele, R. L. Langenfelds, R. J. Francey, J. M. Barnola, and V. I. Morgan, *J. Geophys. Res. Atmos.* 101, 4115 **(1996)**.
5. M. R. Raupach and J. G. Canadell, Observing the Continental Scale Greenhouse Gas Balance of Europe, edited by H. Dolman, R. Valentini, A. Freibauer, Springer, Berlin **(2007)**.
6. A. Fujishima and K. Honda, *Nature* 238, 37 **(1972)**.
7. K. Domen, A. Kudo, T. Onishi, N. Kosugi, and H. Kuroda, *J. Phys. Chem.* 90, 292 **(1986)**.
8. J. Ye, Z. Zou, H. Arakawa, M. Oshikiri, M. Shimoda, and A. Matsushita, *J. Photochem. Photobiol., A* 148, 79 **(2002)**.
9. S. Anandan and J. Wu, *Mater. Lett.* 63, 2387 **(2009)**.
10. L. Zhang, W. Wang, J. Yang, Z. Chen, W. Zhang, L. Zhou, and S. Liu, *Appl. Catal. A-Gen.* 308, 105 **(2006)**.
11. Y. Liu, Z. Wang, B. Huang, K. Yang, Z. Zhang, X. Qin, and Y. Dai, *Appl. Surf. Sci.* 257, 172 **(2010)**.
12. W. Li, *Mater. Chem. Phys.* 99, 174 **(2006)**.
13. W. Du, X. Qian, X. Niu, and Q. Gong, *Adv. Mater.* 7, 2733 **(2007)**.
14. M. Yu, J. Lin, and J. Fang, *Chem. Mater.* 17, 1783 **(2005)**.

Delivered by Ingenta to: National Chung Hsing University
IP: 140.120.25.65
Thu, 20 Oct 2011 04:13:44
AMERICAN SCIENTIFIC PUBLISHERS

15. R. Irmawati, M. N. Noorfarizan Nasriah, Y. H. Taufiq-Yap, and S. B. Abdul Hamid, *Catal. Today* 93, 701 **(2004)**.
16. V. Fruth, M. Popa, D. Berger, C. M. Ionica, and M. Jitianu, *J. Eur. Ceram. Soc.* 24, 1295 **(2004)**.
17. J. Zhu, S. Wang, J. Wang, D. Zhang, and H. Li, *Appl. Catal. B-Environ.* 102, 120 **(2011)**.
18. X. Liu., H. Cao, and J. Yin, *Nano Res.* 4, 470 **(2011)**.
19. K. Yao and H. Zeng, *J. Phys. Chem. C* 111, 13301 **(2007)**.
20. C. C. Chen, R. S. Chen, T. Y. Tsai, Y. S. Huang, D. S. Tsai, and K. K. Tiong, *J. Phys-Condens Mat.* 16, 8475 **(2004)**.
21. J. H. Yan, Y. R. Zhu, Y. G. Tang, and S. Q. Zheng, *J. Alloy Compd.* 472, 429 **(2009)**.

Received: 1 August 2011. Accepted: 12 January 2012.

Delivered by Ingenta to:
National Chung Hsing University
IP : 140.120.25.65
Thu, 04 Oct 2012 01:13:44